The impact of tropical convection and cirrus on upper tropospheric humidity: A Lagrangian analysis of satellite measurements

Brian J. Soden

Geophysical Fluid Dynamics Laboratory, NOAA, Princeton, New Jersey, USA

Received 10 July 2004; revised 25 August 2004; accepted 27 September 2004; published 21 October 2004.

[1] Geostationary satellite observations are used in conjunction with an objective pattern-tracking algorithm to describe the Lagrangian evolution of convection, clouds and water vapor in the tropical upper troposphere. This analysis reveals that larger convective events within a Lagrangian air mass are associated with larger and longer-lived cirrus anvil shields. Convective systems which generate larger cirrus shields are, in turn, associated with higher downstream humidity levels following the anvil's dissipation. In the absence of cirrus, the clear-sky upper troposphere is shown to dry at a rate consistent with radiatively-driven subsidence. The presence of cirrus anvils following a convective event is shown to reduce the rate of drying and for large anvils can even change its sign. Analysis of the Lagrangian tendencies suggests that this moistening effect is not attributable to the evaporation of cirrus condensate, but instead results from the same dynamical mechanisms responsible for the formation and maintenance of the cirrus anvil. *INDEX TERMS:* 3314 Meteorology and Atmospheric Dynamics: Convective processes; 3309 Meteorology and Atmospheric Dynamics: Climatology (1620); 3360 Meteorology and Atmospheric Dynamics: Remote sensing. **Citation:** Soden, B. J. (2004), The impact of tropical convection and cirrus on upper tropospheric humidity: A Lagrangian analysis of satellite measurements, *Geophys. Res. Lett.*, *31*, L20104, doi:10.1029/2004GL020980.

1. Introduction

[2] Understanding the processes which control the water budget of the tropical upper troposphere is essential for the successful modeling of the Earth's climate. The feedbacks from upper tropospheric water vapor and cirrus represent some of the most important and most controversial within the climate system [*Ramanathan and Collins*, 1991; *Lindzen et al.*, 2001; *Held and Soden*, 2000]. While the evaporation of cloud condensate has been shown to be critical in determining the distribution of upper tropospheric moisture in simple models of tropical convection [*Sun and Lindzen*, 1993; *Renno et al.*, 1994; *Emanuel and Pierrehumbert*, 1996], such processes are treated simplistically in current GCMs. On the other hand, diagnostic studies indicate that the observed humidity distribution can be explained primarily through large-scale advection of convectively-saturated air, suggesting little role for the evaporation of cloud condensate [*Salathe and Hartmann*, 1997; *Dessler and Sherwood*, 2000].

This paper is not subject to U.S. copyright.
Published in 2004 by the American Geophysical Union.

[3] Traditionally, the study of convective-cloud-humidity relationships has been approached from a fixed Eulerian perspective whereby spatial or temporal analyses are performed on data sets in a stationary grid [e.g., *Fu et al.*, 1990; *Soden and Fu*, 1995; *Stephens et al.*, 1996; *Hartmann et al.*, 2001; *Allan et al.*, 2002]. However, the rapid temporal sampling provided by geostationary satellites offers the opportunity to track the movement and evolution of cloud and water vapor structures on hourly time scales [*Chen and Houze*, 1997; *Boer and Ramanathan*, 1997; *Soden*, 1998; *Wilcox and Ramanathan*, 2003; *Lou and Rossow*, 2004]. By analyzing satellite data within a moving Lagrangian framework, the evolution of individual cloud systems can be followed and studied over their lifecycle.

2. Data and Methodology

[4] This study uses hourly observations of 6.7 μm "water vapor" ($T_{6.7}$) and 11 μm "window" (T_{11}) brightness temperatures from GOES-7 in conjunction with an objective pattern-tracking algorithm to examine the co-evolution of convection, clouds and water vapor from a Lagrangian perspective. A brief description of the relevant aspects of the GOES data, tracking algorithm, and upper tropospheric humidity retrieval are provided below. For complete details the reader is referred to *Soden* [1998, and references therein].

2.1. Radiance Pattern Tracking

[5] Lagrangian trajectories of tropical convective systems are tracked by matching spatial patterns in 6.7 μm water vapor radiances from successive satellite images. The tracking algorithm is initiated by defining a "target" box of $\sim$(400 km)^2 on the initial image ($t = \tau$) which contains the spatial pattern of pixel-level radiances ($\sim$8 km resolution) to be searched for on the ensuing image ($t = \tau + 1$ hr). The target box is compared with all boxes on the later image within a $\sim$500 km radius, and the box containing the highest spatial correlation defines the "destination" box. Once the destination box is determined, the match is verified by using the destination box to define a new target and performing a reverse (i.e., backwards in time) pattern search. The philosophy behind the reverse pattern search is that the pattern displacement should be independent of which image (i.e., which time) is used to define the reference box and that only a valid match will provide the same displacement for both directions.

[6] Trajectories are constructed by applying the tracking algorithm in a serial fashion. Starting from an initial target box at time ($t = 0$) the tracking algorithm searches for the highest spatial correlation between this pattern and all possible destinations 1 hour later ($t = 1$). If this pattern

search is successful, the destination box at time t = 1 now becomes the new target box and the algorithm searches for the highest spatial correlation between this pattern and all possible destinations at time (t = 2). A trajectory is then constructed by repeating this procedure sequentially throughout a 48 hour period. Complete details regarding the tracking algorithm, its validation and error characteristics are provided by *Soden* [1998].

2.2. Synchronization of Convective Events

[7] To facilitate the analysis of the convective lifecycle, the trajectories are first screened for convective events and then synchronized to a common reference time. The minimum (coldest 1%) 11 μm brightness temperatures ($T_{b\text{-}min}$) are computed at each time in the trajectory calculation. A convective event is deemed to occur whenever $T_{b\text{-}min} < 220$ K. While this threshold is somewhat arbitrary, the results presented below are not sensitive to reasonable changes in its value. All trajectories containing convective events are saved for ±24 hours before and after the convective event, and then synchronized such that the time of coldest $T_{b\text{-}min}$ is set to t = 0. Finally, the resulting synchronized trajectories are screened to discard instances of multiple convective events within the same 48-hour period. For the GOES-7 domain under consideration here (30N–30S, 130W–30W) this procedure yields ~2000 valid trajectories during the period of study (August 1–30, 1987).

2.3. Deep Convection, Cirrus Anvils and Upper Tropospheric Relative Humidity

[8] Following previous studies [*Fu et al.*, 1990; *Chen and Houze*, 1997] we define the deep convective cloud cover (DCC) as the percentage of pixels in the tracking box for which $T_{11} < 220$ K and cirrus anvil cloud cover (CAC) as the percentage of pixels for which $T_{11} < 260$ K. The vertically-averaged upper tropospheric relative humidity (UTH) is estimated from the cloud-free pixels of $T_{6.7}$ within each trajectory box following the method of *Soden and Bretherton* [1993]. Since clouds strongly attenuate the upwelling radiance at 6.7 μm, estimation of UTH is only possible from cloud-free pixels. The 6.7 μm radiances are classified as cloud-contaminated when $T_{11} - T_{6.7} < 25$ K [*Soden*, 1998].

3. Results

3.1. Lagrangian Trajectory Composites

[9] The Lagrangian evolution of DCC, Tb11, CAC, and UTH averaged from the synchronized trajectories is shown in Figure 1. The time axis spans 24 hours before and after the peak in convective activity (defined to be t = 0 see section 2.2). As might be expected, the DCC peaks at t = 0. That is the peak in convective cloud cover coincides with the time at which the coldest 1% of the Tb11 within the tracking box are at their minimum. However, the *mean* Tb11 averaged over all pixels within the tracking box does not reach a minimum until ~2 hours later. This lag reflects the anvil spreading time-scale for tropical convective events and is consistent with the 1–2 hour delay in the peak of CAC (Figure 1, bottom). Also note that the build-up and dissipation of DCC is fairly symmetric about its peak (at t = 0), whereas CAC shows a distinctly skewed evolution with the decay time being roughly twice as long as its formation.

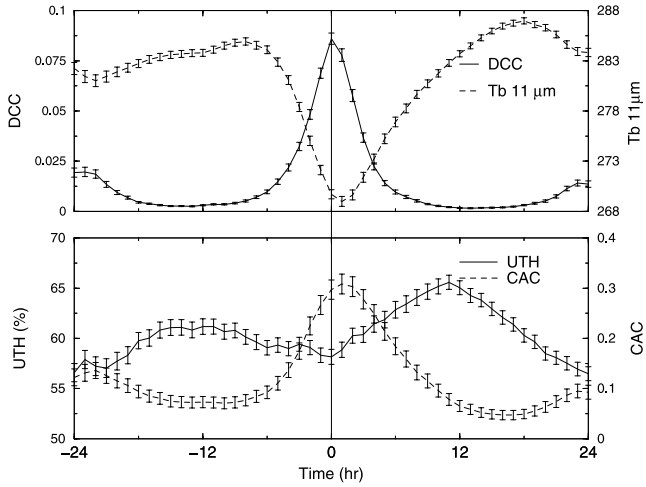

Figure 1. The Lagrangian evolution of DCC (top, solid), Tb11 (top, dashed), CAC (bottom, dashed) and UTH (bottom, solid) within the tracking box averaged from all synchronized trajectories. The time axis spans 24 hours before and after the peak in convective activity (defined as t = 0; see text for details). The vertical bars depict the standard errors of the means.

[10] Interestingly, the clear-sky UTH is at a local minimum during the peak of convection (t = 0) and does not reach its maximum value until almost 12-hours later, well after CAC peaks. There are two possible explanations for the delayed peak in UTH. One is that it results from a moistening of the environmental air due to the evaporation of cirrus condensate following a convective event. However, since UTH is only available from cloud-free pixels, it is also possible that the lag between CAC and UTH is attributable to a cloud-masking effect. As cirrus shields evaporate, more pixels will become cloud-free and, assuming cloudy pixels are more humid than the surrounding environment, the reduction in CAC could lead to an apparent increase in UTH. The relationships between the evolution of CAC and UTH are explored in more detail below.

3.2. Effects of Convective and Cirrus Anvil Coverage

[11] In this section we assess the extent to which the amount of cirrus coverage or subsequent moistening of the upper troposphere depends upon the intensity of the convective event which generated it. To do so we use the fractional coverage of DCC at t = 0 ($DCC_{t=0}$) as a measure of the intensity of convection. The $DCC_{t=0}$ is then compared with the maximum value of CAC or UTH along the trajectory following the convective event (denoted as CAC_{max} or UTH_{max} respectively). To illustrate this dependence, the values of CAC_{max} and UTH_{max} within each trajectory are binned according to the amount of $DCC_{t=0}$, and the average is computed for each bin.

[12] Figure 2a displays the average value of CAC_{max} and UTH_{max} as a function of $DCC_{t=0}$. The amount of anvil coverage increases in proportion to the size of the convective event; i.e., a two-fold increase in $DCC_{t=0}$ results in roughly a two-fold increase in CAC_{max}. The upper

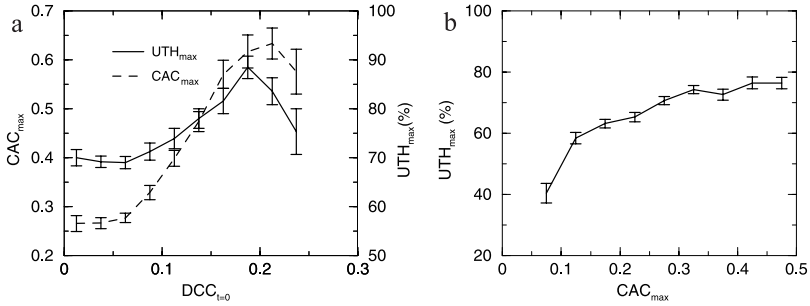

Figure 2. (a) The maximum downstream value of cirrus anvil coverage (CAC_{max}) and upper tropospheric humidity (UTH_{max}) binned as a function of the corresponding fraction of deep convective cloud cover (at t = 0); and (b) the UTH_{max} binned as a function of the corresponding value of CAC_{max}. The results are computed individually for each trajectory and then averaged over all trajectories. The mean and standard error (vertical bar) are plotted for each bin.

tropospheric humidity exhibits a weaker, but qualitatively similar dependence upon the convective intensity. Thus, on average, larger convective events are associated with larger downstream production of cirrus anvils and a greater subsequent moistening of the upper troposphere. When UTH_{max} is binned as a function of the corresponding value of CAC_{max} (Figure 2b), we find that changes in CAC_{max} are associated with roughly twice as large a range in UTH_{max} ($\sim$40% to 80%) as are changes in $DCC_{t=0}$ ($\sim$70% to 90%). That is, the peak value of downstream humidity appears to be more strongly tied to the maximum extent of cirrus anvil coverage during the cloud lifecycle, than to the size of the convective event. This suggests that either the detrained vapor increases as the anvil condensate does or that the evaporation of anvil condensate itself provides an important source of vapor for the upper troposphere.

3.3. Lagrangian Humidity Tendencies

[13] To further explore the relationship between cirrus anvil formation and upper tropospheric moisture we consider the Lagrangian tendencies in UTH. The Lagrangian tendencies are determined from the change in UTH within a given trajectory box as it is tracked from one image to the next and, following *Soden* [1998], are expressed in terms of the fractional change in UTH; i.e., $\Delta \ln UTH = \ln UTH(t = \tau + 1\ \text{hr}) - \ln UTH(t = \tau)$. To eliminate the effects of a change in cloud masking on the UTH tendency, $\Delta \ln UTH$ is computed from only those pixels which are cloud free at both $t = \tau$ and $t = \tau + 1$ hr. This difference measures the relative change in UTH experienced by the layer as it moves horizontally along a trajectory. Note that the trajectory is not a true 3-dimensional Lagrangian depiction of the moisture transport, but rather represents the horizontal movement of a deep layer of upper tropospheric moisture. Since typical subsidence rates ($\sim$1 hPa/hr) are small relative to the depth of the UTH layer ($\sim$400 hPa), the vertical advection of moisture has little impact on the UTH tendency over the 1 hr tracking interval.

[14] To determine whether the Lagrangian tendencies in humidity are modified by the presence of cirrus clouds, the changes in UTH are binned as a function of CAC. The average and standard error of $\Delta \ln UTH$ and the number of observations for each CAC bin are plotted in Figure 3a. For tracking intervals in which the CAC coverage is small (<0.2) the clear-sky UTH decreases over time, and under clear-skies approaches a fractional drying rate of approximately 0.01/hr and agrees with that found by *Soden* [1998]. Following *Soden* [1998] and assuming a typical clear-sky radiative cooling rate of -1.5 K d^{-1}, the subsidence necessary to explain the observed drying rates range is $\sim$20 hPa d^{-1} which is consistent with observed values. As the amount of CAC within the trajectory box increases, the drying rate decreases until it eventually changes sign. For trajectories with CAC > 0.3, $\Delta \ln UTH > 0$ indicating that the upper troposphere tends to moisten with time in the presence of significant CAC.

[15] The relationship between UTH and CAC is further explored in Figure 3b by comparing the UTH tendency as a function of the change in CAC over the 1-hour tracking interval (ΔCAC). This analysis shows that the UTH tendency depends upon both the sign and magnitude of ΔCAC. Trajectory intervals which exhibit the largest

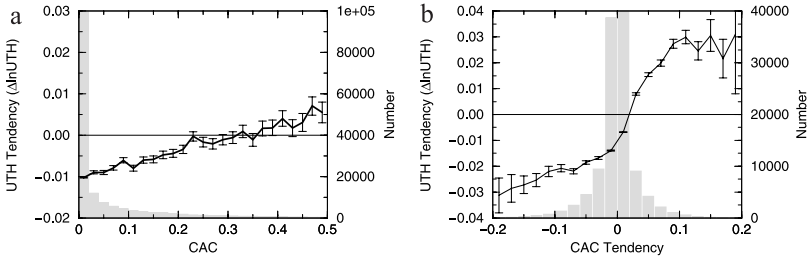

Figure 3. (a) The one-hour Lagrangian tendency in UTH (ΔlnUTH) binned as a function of the fraction of cirrus anvil coverage (CAC). (b) The ΔlnUTH binned as a function of the corresponding one-hour Lagrangian tendency in cirrus anvil coverage (ΔCAC). The mean and standard error (vertical bar) are plotted for each bin. The gray shading depicts the number of observations in each bin.

decrease in CAC coverage also experience the strongest drying rates (~0.03/hr), whereas trajectory intervals with the largest increase in CAC coverage experience the strongest moistening rates. Also note that the strength of the dependence of ΔlnUTH on ΔCAC is much larger than it is with CAC, further underscoring the connection between CAC tendency and UTH tendency. Repeating these calculations using a 3 hr integrated tendency leads to similar results, indicating that the interpretations drawn here are not sensitive to the length of the time increment used.

[16] If cirrus condensate was an important source of moisture for the upper troposphere, one would expect to see increased humidification during periods in which the cirrus decay was most rapid. The fact that decaying cirrus anvils are associated with enhanced drying of the upper troposphere suggests that the evaporation of cirrus condensate does *not* play a significant role in directly modifying the vapor budget of the upper troposphere. Moreover, the largest moistening rates occur when cirrus anvil growth is also greatest, suggesting that the vapor budget is primarily influenced by the same dynamical mechanisms that govern the formation and dissipation of the cirrus anvil rather than through the evaporation of condensate.

4. Discussion

[17] In this study, hourly radiance observations from geostationary satellites are used in conjunction with an objective pattern-tracking algorithm to describe the Lagrangian co-evolution of convection, clouds and water vapor in the tropical upper troposphere. This analysis shows that stronger convective events are, on average, associated with larger and longer-lived cirrus anvil shields. Convective systems which generate larger cirrus shields are, in turn, associated with higher ''downstream'' humidity levels following the anvil's dissipation. In the absence of significant cirrus coverage, the clear-sky upper troposphere is shown to dry at a rate consistent with radiatively-driven subsidence. However, the presence of cirrus anvils following a convective event is shown to be associated with a moistening of the adjacent clear-sky upper troposphere, but this moistening effect depends strongly on whether the cirrus anvils are in a growth or decay phase.

[18] The analysis indicates that periods of cirrus decay are associated with enhanced drying of the upper troposphere, while periods of cirrus growth are associated with enhanced moistening. This suggests that the increased humidification that is observed in association with cirrus likely results from the same vertical-transport processes responsible for the formation and maintenance of the cirrus, such as convective detrainment of vapor or the modification of radiatively-driven subsidence rates [*Sherwood*, 1999], rather than through the direct evaporation of cirrus condensate [*Sun and Lindzen*, 1993; *Renno et al.*, 1994]. Such an interpretation is consistent with diagnostic analyses [*Salathe and Hartmann*, 1997; *Dessler and Sherwood*, 2000] which indicate that the distribution of upper tropospheric water vapor can be explained primarily through the large-scale advection of saturated air without accounting for re-evaporation of cloud condensate. It also supports the assertion by *Lou and Rossow* [2004] that the amount of ice water contained in cirrus clouds is too small to play a significant role in modifying the moisture budget of the upper troposphere. Finally, it also is consistent with GCM simulations which indicate that the vapor budget of the tropical upper troposphere is insensitive to changes in the mass of convectively-detrained cirrus condensate [*Clement and Soden*, 2004].

References

Allan, R. P., A. Slingo, and M. A. Ringer (2002), Influence of dynamics on the changes in tropical cloud radiative forcing during the 1998 El Niño, *J. Clim.*, *15*, 1979–1986.

Boer, E. R., and V. Ramanathan (1997), Lagrangian approach for deriving cloud characteristics from satellite observations, *J. Geophys. Res.*, *102*, 21,383–21,399.

Chen, S. S., and R. A. Houze Jr. (1997), Diurnal variation and life-cycle of deep convective systems over the tropical Pacific warm pool, *Q. J. R. Meteorol. Soc.*, *123*, 357–388.

Clement, A. C., and B. J. Soden (2004), The sensitivity of the tropical-mean radiative energy budget, *J. Clim.*, in press.

Dessler, A. E., and S. C. Sherwood (2000), Simulations of tropical upper tropospheric humidity, *J. Geophys. Res.*, *105*, 20,155–20,163.

Emanuel, K. A., and R. T. Pierrehumbert (1996), Microphysical and dynamical control of tropospheric water vapor, in *Clouds, Chemistry, and Climate*, *NATO ASI Ser. 1 Global Environ. Change*, vol. 35, edited by P. J. Crutzen and V. Ramanathan, pp. 17–28, Springer-Verlag, New York.

Fu, R., A. D. Del Genio, and W. B. Rossow (1990), Behavior of deep convective clouds in the tropical Pacific deduced from ISCCP radiances, *J. Clim.*, *3*, 1129–1152.

Hartmann, D. L., L. A. Moy, and Q. Fu (2001), Tropical convection and the energy balance at the top of the atmosphere, *J. Clim.*, *14*, 4495–4511.

Held, I. M., and B. J. Soden (2000), Water vapor feedback and global warming, *Annu. Rev. Energy Environ.*, *25*, 441–475.

Lindzen, R. S., M. D. Chou, and A. Y. Hou (2001), Does the Earth have an adaptive infrared iris?, *Bull. Am. Meteorol. Soc.*, *82*, 417–432.

Lou, Z., and W. B. Rossow (2004), Characterizing tropical cirrus lifecycle, evolution and interaction with upper tropospheric water vapor using a Lagrangian trajectory analysis of satellite observations, *J. Clim.*, in press.

Ramanathan, V., and W. Collins (1991), Thermodynamic regulation of ocean warming by cirrus clouds deduced from observations of the 1987 El Niño, *Nature*, *351*, 27–32.

Renno, N. O., K. A. Emanuel, and P. H. Stone (1994), Radiative convective model with an explicit hydrologic cycle, *J. Geophys. Res.*, *99*, 14,429–14,441.

Salathe, E. P., and D. L. Hartmann (1997), A trajectory analysis of tropical upper tropospheric moisture and convection, *J. Clim.*, *10*, 2533–2547.

Sherwood, S. C. (1999), On moistening of the tropical troposphere by cirrus clouds, *J. Geophys. Res.*, *104*, 11,949–11,960.

Soden, B. J. (1998), Tracking upper tropospheric water vapor radiances: A satellite perspective, *J. Geophys. Res.*, *103*, 17,069–17,081.

Soden, B. J., and F. P. Bretherton (1993), Upper tropospheric relative humidity from the 6.7 μm channel: Method and climatology for July 1987, *J. Geophys. Res.*, *98*, 16,669–16,688.

Soden, B. J., and R. Fu (1995), A satellite analysis of deep convection, upper tropospheric humidity and the greenhouse effect, *J. Clim.*, *8*, 2333–2351.

Stephens, G. L., D. L. Jackson, and I. Wittmeyer (1996), Global observations of upper-tropospheric water vapor derived from TOVS radiance data, *J. Clim.*, *9*, 305–326.

Sun, D. Z., and R. S. Lindzen (1993), Distribution of tropical tropospheric water vapor, *J. Atmos. Sci.*, *50*, 1644–1660.

Wilcox, E. M., and V. Ramanathan (2003), Spatial and temporal scales of precipitating tropical cloud systems in satellite imagery and the NCAR CCM3, *J. Clim.*, *16*, 3545–3559.

B. J. Soden, Geophysical Fluid Dynamics Laboratory, NOAA, P. O. Box 308, Princeton, NJ 08542, USA. (brian.soden@noaa.gov)